Transactions of the Royal Society of Edinburgh: Earth Sciences, **95**, 265–276, 2004

Petrochemical characteristics of felsic veins in mantle xenoliths from Tallante (SE Spain): an insight into activity of silicic melt within the mantle wedge

Yohei Shimizu, Shoji Arai, Tomoaki Morishita, Hisayoshi Yurimoto and Fernando Gervilla

ABSTRACT: Felsic and related veins within mantle-derived peridotite xenoliths from Tallante, Spain, were examined in order to understand the mantle-wedge processes related to the behaviour of Si-rich melt. The thickest part of the vein has a quartz diorite lithology, and is composed mainly of quartz and plagioclase, with pyroxenes, hydrous mineral, apatite, zircon and rutile present as minor phases. The thinner parts are free of quartz and predominantly composed of plagioclase. Orthopyroxene always intervenes between the internal part (plagioclase ± quartz) and host peridotite, indicating that it is a product of interaction between silica-oversaturated melt and olivine. This indicates that a sufficiently high melt/wall rock ratio enabled the melt to retain its silica-oversaturated character.

The quartz diorite part has adakite-like geochemical signatures, except for negative Ba, Rb Eu and Sr anomalies, and positive Th and U anomalies. These negative anomalies indicate that fractionation of plagioclase and hydrous minerals was achieved between the upper most mantle and the slab melting zone. The shape of the rare-earth element (REE) pattern of clinopyroxene in quartz diorite is strikingly similar to that of clinopyroxene phenocrysts from Aleutian adakites. However, the former has one order higher REE contents than the latter, except for Eu which shows a prominent negative spike. This feature was caused by the precipitation of large amounts of plagioclase and small amounts of clinopyroxene from a fractionated adakitic melt before and during solidification. This adakitic melt was produced by partial melting of a detached and sinking slab beneath the Betic area in the Tertiary.

KEY WORDS: Adakite, orthopyroxene, peridotite xenolith, quartz diorite.

The origin of the continental crust is an important problem for our understanding of the Earth's history. It has been controversial, and many workers have discussed the highly specific structure and composition of the continental crust (e.g. Taylor & McLennan 1985; Rudnick & Fountain 1995). Taylor & McLennan (1985) suggested an andesitic composition for the continental crust. Kelemen (1995) more recently pointed out that the continental crust is similar in composition to high-Mg andesites, and suggested that the high-Mg andesitic character has been achieved by melt/rock reaction in the upper mantle based on experimental constraints and phase equilibra calculations. Tatsumi (2000a, b) examined the roles of slab melting and delamination of the lower crust by means of geochemical modelling, and concluded that the delamination process has been important in the formation of the continental crust.

Defant & Drummond (1990) described the adakites as volcanic rocks derived from partially molten oceanic slab. Adakite has high Al_2O_3 wt.%, positive Sr anomaly, and high Sr/Y and La/Yb ratios compared with normal arc magma. The adakitic melt occurs in a specific setting where hot and/or young oceanic plate is subducted. Experimental studies have demonstrated that the melting of downgoing oceanic slab can produce melts similar to adakite in composition (Rapp *et al*. 1991; Sen & Dunn 1994; Rapp & Watson 1995; López & Castro 2001). Defant & Drummond (1990) also pointed out the similarities between adakite and high-Al tonalite, trondhjemite and granodiorite (TTG). The high-Al TTG is a major component of Archaean crust and is possibly formed by slab melting as a result of a higher geothermal gradient during the Archaean. This hypothesis is a plausible explanation for the origin of the Archaean continental crust. However, there are also compositional differences between them: the adakites generally have a higher MgO content than the experimentally duplicated slab melt and high-Al TTG (Rapp *et al*. 1999; Martin 1999; Smithies 2000). This is because of the assimilation and fractional crystallisation (mantle AFC) of slab melts during its ascent through the mantle, as suggested both by natural (Kay *et al*. 1993) and experimental adakite studies (Rapp *et al*. 1999).

There is little information related to the slab-melt activity within the mantle from mantle peridotite studies because of the scarcity of mantle xenoliths derived from the mantle wedge. Recently, Arai *et al*. (2003) reported quartz diorite veining in a mantle peridotite xenolith from Tallante, SE Spain. The relationship between the peridotite and such a felsic vein provides an indication of how the slab melt ascends through the mantle wedge.

In this paper, the present authors describe detailed petrochemical characteristics of the quartz diorite and related veinlets from mantle xenoliths of Tallante, SE Spain, in order to explore the behaviour of slab melts within the mantle wedge.

https://doi.org/10.1017/S0263593300001061 Published online by Cambridge University Press

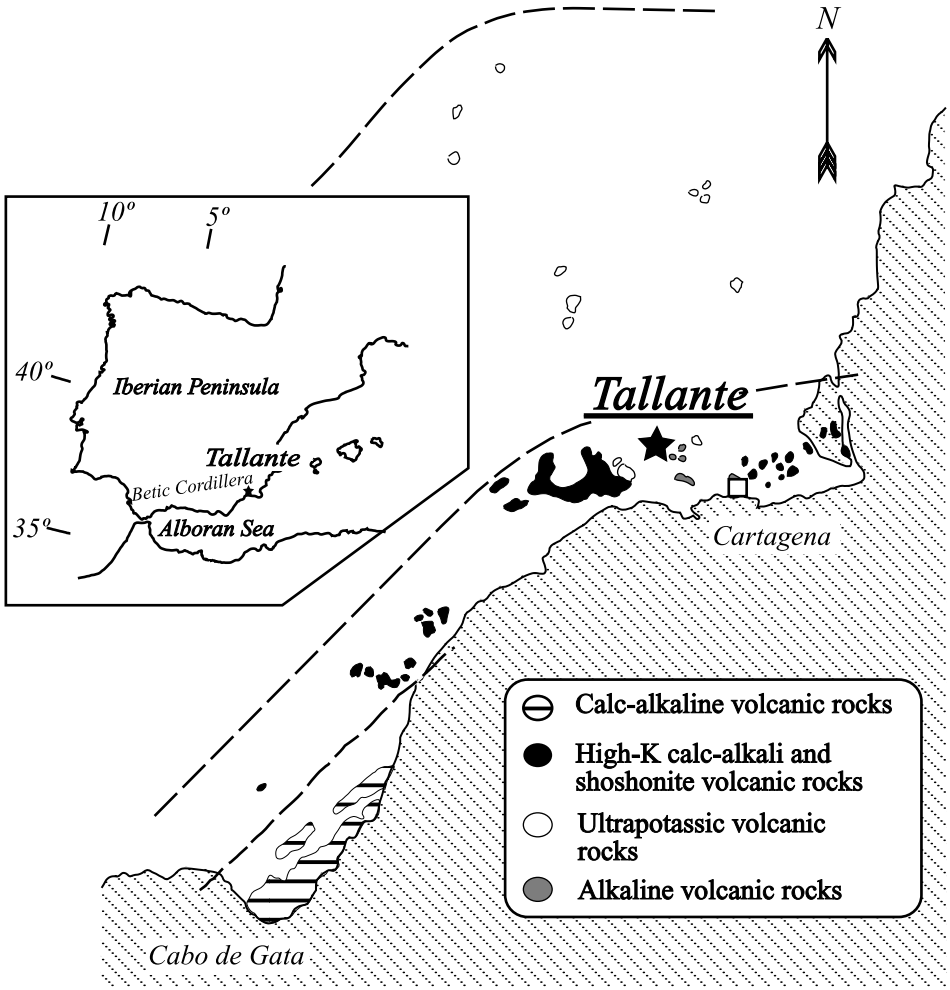

Figure 1 Locality map of Tallante, SE Spain. The distribution of Tertiary volcanic rocks around Tallante is after Ancochea & Nixon (1987). The K content of the volcanic rocks systematically increases northward.

1. Geological background and petrography of peridotite xenoliths

The Neogene volcanic rocks in SE Spain (Fig. 1) consist of calc-alkaline, high-K calc-alkaline, shoshonite, ultrapotassic rocks (lamproite) (Venturelli *et al.* 1988) and alkali basalts (López-Ruiz & Rodoríguez-Badiola 1980). The composition and eruptive age of the calc-alkaline rocks regularly change northward; their K_2O content increases considerably northward (e.g. Ancochea & Nixon 1987). This relationship has been interpreted as a result of northward subduction of slab in the Alboran Sea at the end of Oligocene (Araña & Vegas 1974). The seismic tomography indicates that there possibly is a detachment slab beneath the region (Blanco & Spakman 1993). Turner *et al.* (1999) ascribed the calc-alkaline and related magmas to anatexis of lithosphere beneath the Betic region.

The alkali basalt in Tallante (NW Cartagena, Province of Murcia) includes abundant mantle-derived ultramafic xenoliths (e.g. Dupuy *et al.* 1986; Ancochea & Nixon 1987; Capedori *et al.* 1989). These ultramafic xenoliths occur as rounded or elliptically shaped ejecta within host alkali-basaltic pyroclastics. The ultramafic xenoliths are less than 25 cm in diameter, and they are predominantly lherzolite and harzburgite and occasionally pyroxenites. The ultramafic xenoliths are classified into two types, Groups I and II in the sense of Frey & Prinz (1978). Group I comprises lherzolite, harzburgite and pyroxenites, while Group II is hornblende-bearing clinopyroxenite. Rocks of both groups sometimes form composite xenoliths (Irving 1980). Group I rocks can further be divided into two types; namely, spinel peridotite and plagioclase peridotite in mineral assemblage. Group I peridotites have equigranular texture and, in a rare case, porphyroclastic texture with olivine porphyroclast (cf. Mercier & Nicolas 1975). Olivine and pyroxenes often show kink bands and pyroxenes contain exsolution lamellae. Pyroxenes show more prominent exsolution lamellae in plagioclase peridotite than in spinel peridotite. Plagioclase, which shows slight chemical zoning, is observed as an interstitial phase, especially surrounding grains of spinel. Hydrous minerals (amphibole and mica) are rarely found as interstitial grains, although substantial amounts of hydrous minerals (amphiboles and rarely mica) with plagioclase occur along the contact between Group I and II rocks of the composite xenoliths. Group I rocks occasionally contain lenticular fine-grained aggregates of pyroxenes and spinel (Fig. 2). Group II rocks have igneous textures, and their mineral assemblage is clinopyroxene+amphibole+magnetite, with or without phlogopite, olivine and orthopyroxene.

2. Petrography of the quartz diorite and related veins

Peridotites from Tallante are characterised by secondary, white, network-like veins (Fig. 2; Arai *et al.* 2003), which are less than 8 mm in thickness, and cut or replace primary minerals. Each vein is mainly composed of plagioclase, and modal quartz can be found only at the thick (>1 mm) parts of

https://doi.org/10.1017/S0263593300001061 Published online by Cambridge University Press

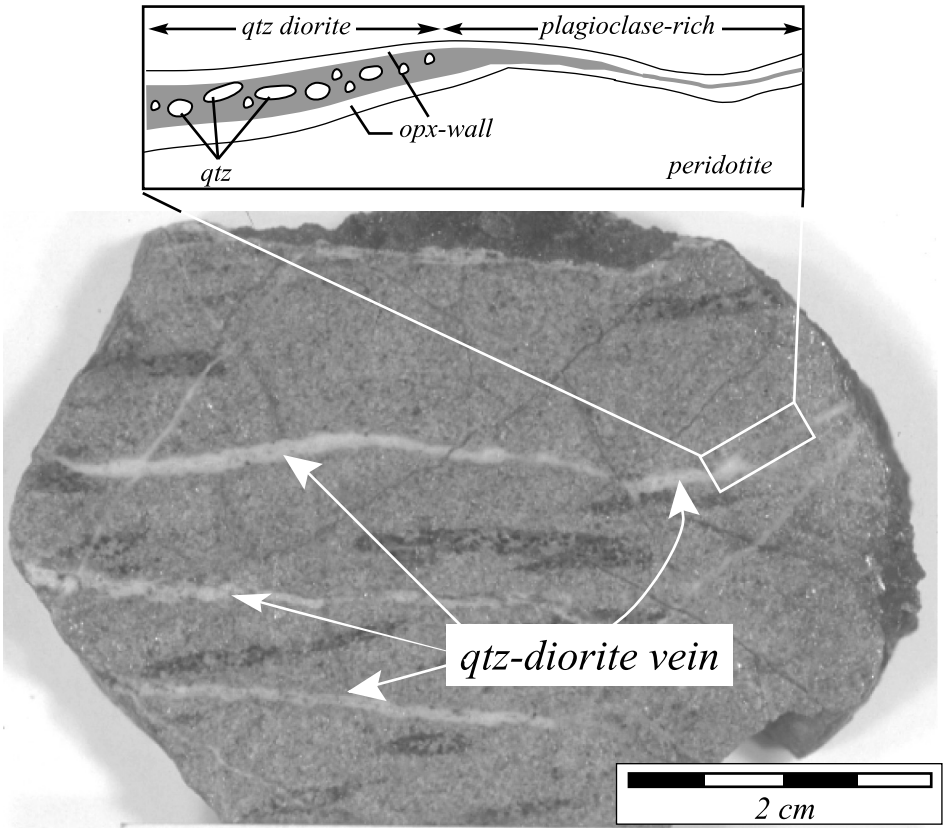

Figure 2 Sawed surface of the peridotite xenolith penetrated by a network of white veins, which are mainly composed of plagioclase. Quartz is found only in thick (>1-mm) parts, which have quartz diorite lithology. Foliation is defined by dark lenticular aggregates of spinel and pyroxenes: (qtz) quartz; and (opx) orthopyroxene.

the vein, which is quartz diorite, as described below (Fig. 2). Orthopyroxene occurs between olivine of the host peridotite and the internal part (plagioclase ± quartz) (Fig. 3b). In very thin (<0·1-mm) veins, orthopyroxene is sporadically present between plagioclase and olivine (Fig. 3a). Clinopyroxene and orthopyroxene in the host peridotite tend to have more prominent exsolution lamellae when the rock contains plagioclase-rich veins.

The thick part of the veins (=quartz-bearing) reveals important information. It contains small amounts of orthopyroxene, clinopyroxene, amphibole, phlogopite, apatite, rutile, zircon and glass in addition to plagioclase and quartz. The presence of quartz is specially remarkable. In the thickest part, quartz is anhedral, and is usually 100–200 μm, reaching up to 750 μm in diameter. It occurs only at the centre of the vein, and is surrounded by plagioclase and/or glass. The plagioclase is less than 1·5–2 mm in diameter and tends to be coarser toward the centre of the vein. Plagioclase is slightly zoned, and there is no K-feldspar. Apatite, rutile and zircon are observed as inclusions in plagioclase, quartz and/or glass. Rutile and zircon are 10–100 μm across, and rutile is more abundant than zircon. Apatite often occurs as needles in the felsic part of the vein. Glass occurs along the grain boundaries of quartz, plagioclase and orthopyroxene, and never occurs as inclusions. Clinopyroxene is rare, but is very coarse (2 mm across) in the quartz-bearing part of the vein. The coarse clinopyroxene grain is also in contact with quartz and glass, and is partly enclosed by plagioclase. Amphibole and phlogopite are interstitial and rarely show a linear arrangement.

We obtained the modal composition of the quartz-bearing part of the vein by measuring the area of all phases on photomicrographs using image data processing software (NIH image and Adobe Photoshop) (Table 1). Orthopyroxene lining the olivine wall was excluded from this estimate. Quartz and plagioclase occupy more than 90 vol.% of the vein by volume, and are classified as 'quartz diorite' according to the nomenclature of Streckeisen (1976); we adopt the term quartz diorite vein hereafter (Fig. 2).

3. Analytical methods

Minerals and glass were analysed for major elements by a JEOL JXA-8800 electron probe X-ray microanalyser (WDS) at the Centre for Cooperative Research of Kanazawa University, Kanazawa, Japan. Microprobe analysis was conducted with an acceleration voltage of 20 keV and sample currents of 20 nA with a 3-μm probe diameter. Oxides, and natural and synthetic minerals were used as standards. ZAF correction procedure was applied to all raw data. Secondary standards, including olivine, clinopyroxene, spinel and alkali feldspar, were analysed to ensure accuracy for the major elements. The cation fractions of Mg, Fe^{2+}, Al, Cr and Fe^{3+} in spinel were calculated assuming spinel stoichiometry after allotting all of Ti to the ulvöspinel molecule. Selected microprobe analyses are listed in Table 2.

Selected clinopyroxenes were analysed *in situ* for rare-earth elements (REEs), and Ti, Sr, Zr and Y using a Cameca IMS 3f ion-microprobe (SIMS) at the Tokyo Institute of Technology, Tokyo, Japan. The analytical procedure used on the ion microprobe was after Yurimoto *et al.* (1989) and Wang & Yurimoto (1993). Ion microprobe analyses are listed in Table 3.

The present authors tried to determine the trace element composition of the bulk quartz diorite vein. The rock sample with the vein was sliced into thin slabs with a diamond saw. Peridotitic portions around the quartz diorite veins were eliminated first by grinding the cut surface. After that, the

https://doi.org/10.1017/S0263593300001061 Published online by Cambridge University Press

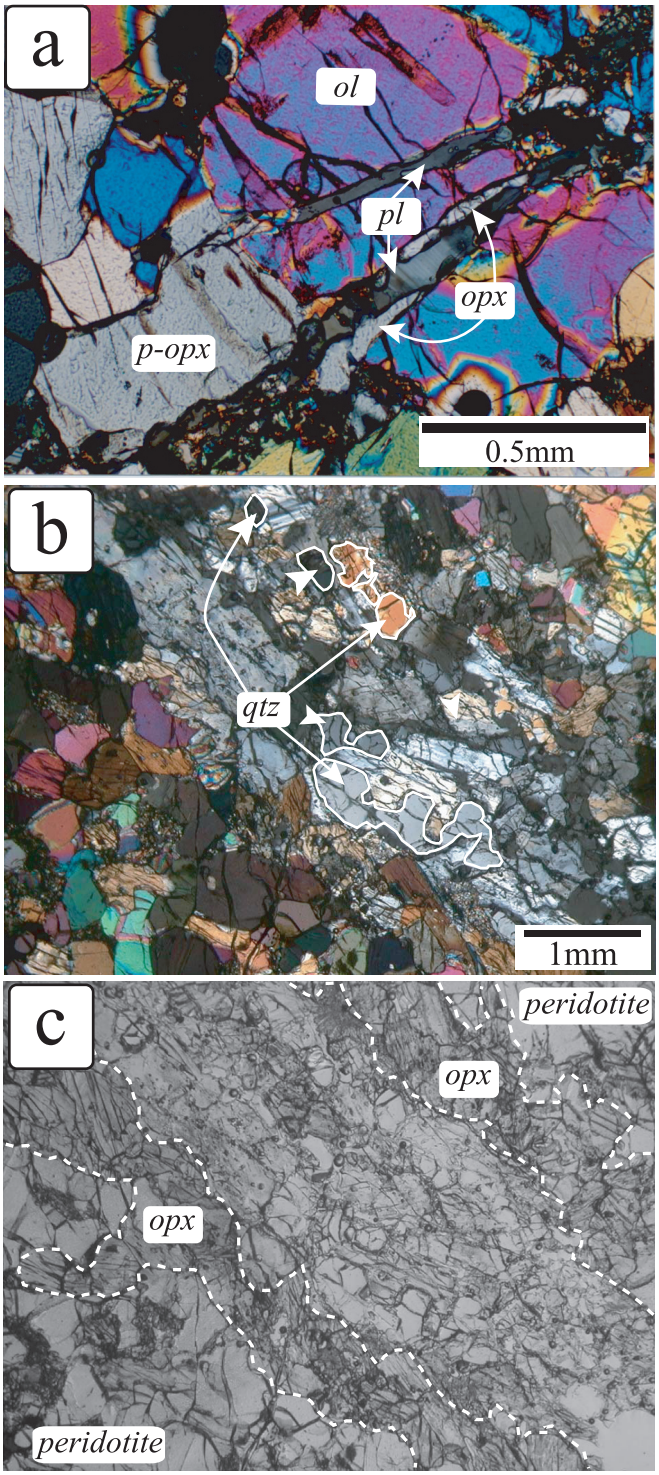

Figure 3 Photomicrographs of secondary veinlets from Tallante, SE Spain: (a) Lherzolite with a thin plagioclase vein associated with orthopyroxene. Primary olivine (ol) and orthopyroxene (p-opx) are cut and replaced by the vein. Note the orthopyroxene (opx) forms between the olivine and plagioclase (pl). Crossed-polarised light. (b) The quartz diorite vein within the peridotite. Note that the quartz grains (qtz) are at the centre of the vein, and thin orthopyroxenite [see (c)] is between the felsic vein and host olivine. Crossed-polarised light. (c) The same as (b), with plane-polarised light. Orthopyroxenite (opx) is highlighted by white broken lines.

remaining fragments were ground to a powder using an agate mortar. They eventually obtained 4 g of powder sample of the vein. The trace-element composition of the vein was determined on fused glass (prepared by mixing the rock powder with one third $LiBO_2$) by laser ablation (193 nm ArF excimer) inductively coupled plasma mass spectrometry (Agilent 7500S) at the Research School of Earth Sciences, Australian National University, Canberra, Australia. Analytical data are listed in Table 4.

Table 1 Modal composition of the quartz-diorite vein determined by the area measured for each phase on photomicrogphs

Modal composition	Quartz diorite vein (vol.%)
Plagioclase	73·46
Quartz	16·91
Orthopyroxene	2·90
Clinopyroxene	2·69
Glass	3·67
Apatite	0·33
Rutile	0·04
Total	100·00

4. Geochemistry

4.1. Olivine and spinel

Peridotites with veins tend to show wider ranges of Fo contents of olivine (=89·3–91·4) and Cr# [=Cr/(Cr+Al) atomic ratio] of spinel (=0·11–0·33) than vein-free peridotites (Fig. 4). However, there is no difference in TiO_2 content and the $Fe^{3+}/(Fe^{3+}+Al^{3+}+Cr^{3+})$ ratio of spinel. The peridotite with the thickest, i.e. quartz diorite, vein has a low Fo content of olivine (=89·9–89·3) and Cr# of spinel (=0·114–0·156), and differs markedly from the peridotites with thinner veins in their olivine-spinel chemical variations (Fig. 4). The Cr# of spinel in the orthopyroxene wall of quartz diorite vein is slightly high (=0·13–0·17) relative to that in the host peridotite (=0·12–0·16), while the $Fe^{3+}/(Al+Cr+Fe^{3+})$ ratio and TiO_2 wt.% are the same.

4.2. Clinopyroxene

The clinopyroxene core in the peridotite with the veins has a relatively homogeneous composition En_{47} Fs_4 Wo_{48} with Al_2O_3 and Cr_2O_3 contents of 5·52–6·32 wt.% and 1·07–1·23 wt.%, respectively. However, it commonly shows chemical zoning; for example, Al_2O_3 wt.% decreases from core (=6·32 wt.%) to rim (=4·65 wt.%), while Cr_2O_3 wt.% slightly increases from core (=0·74 wt.%) to rim (=0·91 wt.%), with a constant Mg# [=100*Mg/(Mg+Fe) atomic ratio] of 92·4–92·7. The TiO_2 content is 0·30–0·74 wt.%. The Na_2O content of clinopyroxene is clearly lower (<0·5 wt.%) in the peridotite with the quartz diorite vein than in that with thin veins (0·5–1wt.%).

The clinopyroxene in the quartz diorite vein is apparently different in composition from the primary clinopyroxenes in peridotites (Fig. 5). It shows an extremely low content of TiO_2 (<0·2 wt.%), Cr_2O_3, Al_2O_3 (=0·71–1·0wt.%) and Na_2O (=0·14–0·20wt.%), and a relatively high CaO content (=22·7–24·1 wt.%) compared with the peridotite clinopyroxenes (Fig. 5; Table 4). A coarse clinopyroxene grain within the quartz diorite vein shows chemical zoning from the interior to the exterior of the vein (Fig. 5). Both Mg# and Al_2O_3 increase from the inside rim (89·9 and 0·74 wt.%, respectively) toward the outside rim (93·2 and 1·04 wt.%, respectively) (Fig. 5).

4.3. Orthopyroxene

Orthopyroxene associated with the veins is apparently lower in Al_2O_3, Cr_2O_3 and CaO contents than ordinary peridotite

https://doi.org/10.1017/S0263593300001061 Published online by Cambridge University Press

Table 2 Selected electron microprobe analyses of constituent minerals and glass in Tallante xenoliths. A glass composition of slab-derived melt from a peridotite xenolith from Batan Island, the Philippines (Schiano *et al.* 1995), is also listed for comparison: (Mg#) Mg/(Mg+Fe) atomic ratio except for spinel [Mg# for spinel is $Mg/(Mg+Fe^{2+})$ atomic ratio, for which Fe^{2+} was calculated assuming spinel stoichiometry]; (Cr#) Cr/(Cr +Al) atomic ratio for spinel; and (An) Ca/(Ca+Na) atomic ratio for plagioclase.

	Olivine							Clinopyroxene									
Rock:														Quartz diorite vein)			
Sample no.	Spinel peridotite (990430–8)	Plagioclase peridotite (990430–7)	Sp peridotite with vein (990806–5)	Pl peridotite with vein (TAL-17)	Peridotite with quartz diorite vein (9901015–8)	Composite xenolith (990806–21)	Group II (990414–20)	Spinel peridotite (990430–8)	Plagioclase peridotite (990430–7)	Spinel peridotite with vein (990806–5)	Plagioclase peridotite with vein (core) (990414–15)	Plagioclase peridotite with vein (rim) (990414–16)	Peridotite with quartz diorite vein (991015–8)	Inside (991015–9)	Outside (991015–10)	Composite xenolith (990806–21)	Group II (990414–20)
SiO_2	40·84	40·54	41·18	40·99	41·23	40·15	38·83	51·59	51·56	53·61	52·70	51·42	51·77	54·92	55·58	51·56	52·92
TiO_2	0·01	0·01	0·01	0·02	0·00	0·03	0·00	0·45	0·63	0·30	0·50	0·48	0·61	0·16	0·10	0·77	0·49
Al_2O_3	0·00	0·01	0·00	0·00	0·04	0·00	0·01	6·16	5·65	4·10	4·65	6·35	4·46	0·74	1·04	5·23	3·27
Cr_2O_3	0·00	0·00	0·01	0·00	0·00	0·00	0·01	1·35	0·95	1·08	1·05	1·04	0·63	0·01	0·05	0·96	0·33
FeO	8·86	9·53	10·27	10·15	10·33	14·27	22·68	1·99	2·19	2·19	2·22	2·22	2·10	3·51	2·40	2·38	6·18
MnO	0·09	0·11	0·16	0·14	0·10	0·20	0·36	0·07	0·04	0·09	0·10	0·06	0·15	0·12	0·03	0·13	0·20
MgO	49·65	49·38	48·92	48·27	48·29	45·52	38·02	15·51	15·40	16·33	15·78	15·09	16·23	17·44	18·45	15·29	14·38
CaO	0·03	0·04	0·04	0·03	0·02	0·06	0·07	21·28	22·16	22·57	23·29	22·82	22·63	23·86	24·08	22·31	20·89
Na_2O	0·00	0·01	0·00	0·00	0·01	0·02	0·02	1·01	0·79	0·66	0·71	0·82	0·46	0·17	0·18	0·77	1·00
K_2O	0·02	0·01	0·00	0·00	0·00	0·00	0·02	0·01	0·02	0·01	0·01	0·03	0·03	0·01	0·02	0·00	0·03
NiO	0·37	0·36	0·38	0·38	0·46	0·31	0·11										
Total	99·86	100·00	100·97	99·98	100·49	100·56	100·13	99·42	99·39	100·94	101·01	100·33	99·07	100·94	101·93	99·40	98·76
Mg#	0·910	0·90	0·894	0·894	0·892	0·850	0·749	0·932	0·926	0·930	0·926	0·923	0·933	0·898	0·932	0·919	0·805
An (Cr#)																	

Table 2 *Continued*.

Rock:	Prthopyroxene											Spinel					
								Quartz diorite vein									
Sample no.	Spinel peridotite (990430–8)	Plagioclase peridotite (990430–7)	Spinel peridotite with vein (990806–3)	Spinel peridotite with vein (vein) (990806–3)	Plagioclase peridotite with vein (TAL17)	Plagiolcase peridotite with vein (vein) 990806–26)	Peridotite with quartz diorite vein (9901015–8)	Core (991015–8)	Rim (991015–8)	Composite xenolith (990806–21)	Group II (990806–16)	Spinel peridotite (990430–8)	Plagioclase peridotite (990430–7)	Spinel peridotite with vein (990806–5)	Plagioclase peridotite with vein (TAL17)	Peridotite with quartz diorite vein (quartz)	Composite xenolith (990806–20)
SiO_2	55·94	55·82	56·26	57·78	56·63	56·66	55·56	57·79	57·41	55·14	55·23	0·01	0·02	0·00	0·03	0·02	0·04
TiO_2	0·08	0·11	0·15	0·07	0·23	0·07	0·18	0·10	0·10	0·12	0·06	0·05	0·08	0·11	0·10	0·07	0·09
Al_2O_3	3·31	3·48	3·92	2·09	2·93	2·62	4·69	1·43	1·93	3·46	1·98	49·30	50·88	46·68	40·50	57·21	52·13
Cr_2O_3	0·41	0·50	0·68	0·26	0·60	0·31	0·49	0·04	0·00	0·38	0·00	18·75	16·98	22·95	27·98	11·47	13·78
FeO	5·66	5·97	5·72	5·70	6·47	6·09	6·34	6·93	6·66	7·71	13·87	9·99	10·78	10·33	13·48	10·28	14·26
MnO	0·11	0·09	0·11	0·13	0·15	0·13	0·13	0·10	0·13	0·19	0·35	0·11	0·11	0·12	0·19	0·14	0·18
MgO	33·93	33·06	33·02	34·48	33·16	33·90	32·08	34·66	34·21	32·34	27·94	20·05	20·13	19·88	17·23	21·05	18·69
CaO	0·59	0·70	0·94	0·70	1·05	0·71	1·02	0·28	0·35	0·57	0·91	0·01	0·01	0·00	0·01	0·00	0·01
Na_2O	0·04	0·06	0·03	0·02	0·03	0·03	0·01	0·00	0·00	0·01	0·06	0·00	0·00	0·01	0·00	0·02	0·00
K_2O	0·01	0·01	0·01	0·00	0·02	0·02	0·01	0·04	0·00	0·01	0·02	0·01	0·01	0·03	0·01	0·00	0·00
NiO												0·26	0·31	0·27	0·20	0·39	0·27
Total	100·08	99·80	100·84	101·23	101·27	100·54	100·51	101·37	100·78	99·93	99·34	98·53	99·31	100·38	99·73	100·65	99·44
Mg#	0·914	0·908	0·911	0·915	0·901	0·908	0·900	0·899	0·901	0·882	0·782	0·805	0·799	0·795	0·719	0·807	0·740
An (Cr#)												0·203	0·182	0·248	0·316	0·118	0·150

Rock:	Plagioclase					Amphibole			Phlogopite			Glass			
				Quartz diorite vein								Quartz diorite vein			
Sample no.	Plagioclase peridotite (990430–7)	Plagioclase peridotite with vein (990414–1)	Plagioclase peridotite with vein (vein) (990414–1)	Core (991015–8)	Rim (991015–8)	Plagioclase-rich vein (990806–5)	Composite xenolith (990414–19)	Group II (990414–20)	Plagioclase-rich vein (990414–15)	Composite xenolith (990806–21)	Group II (990414–20)	Inside (991015–8)	Outside (991015–8)	Slab-derived melt (Schiano *et al.* 1995) (IVI)	
SiO_2	55·43	54·40	53·55	54·87	59·22	44·01	42·01	42·00	38·99	38·07	38·52	72·37	67·81	59·69	
TiO_2	0·03	0·01	0·01	0·00	0·01	1·57	4·36	4·00	1·00	3·72	4·44	0·36	0·84	0·12	
Al_2O_3	29·14	29·19	29·12	28·94	25·86	14·04	13·31	12·77	16·69	16·60	14·65	13·37	12·85	18·47	
Cr_2O_3	0·00	0·04	0·00	0·00	0·00	1·76	1·26	0·02	0·28	0·34	0·06	0·04	0·03		
FeO	0·11	0·07	0·17	0·08	0·00	3·10	6·12	9·18	3·22	5·22	9·21	1·22	1·20	2·71	
MnO	0·00	0·00	0·07	0·05	0·00	0·05	0·08	0·11	0·00	0·03	0·05	0·05	0·02	0·11	
MgO	0·03	0·02	0·11	0·03	0·05	18·17	15·46	14·04	22·87	20·89	18·04	2·07	1·81	1·11	
CaO	11·83	11·44	12·24	11·60	9·12	11·94	10·90	10·91	0·01	0·02	0·03	5·13	5·30	4·10	
Na_2O	4·80	4·64	5·35	4·80	5·55	2·98	3·10	2·89	0·82	1·01	0·97	2·16	0·95	5·07	
K_2O	0·04	0·30	0·21	0·36	0·43	0·02	0·86	1·19	9·93	8·39	8·38	0·96	1·11	2·47	
NiO															
Total	101·40	100·11	100·83	100·73	100·25	97·64	97·46	97·11	93·81	94·29	94·36	97·73	91·92	93·85	
Mg#						0·912	0·818	0·731	0·926	0·877	0·777	0·751	0·729	0·422	
An (Cr#)	57·6	57·6	55·8	57·1	47·6										

Table 3 Rare-earth element (REE), Ti, Sr, Zr and Y abundances (p.p.m.) of representative clinopyroxenes in Tallante peridotite xenoliths determined by SIMS.

Rock:	Peridotite with the vein			Quartz diorite vein	Spinel peridotite	Plagioclase peridotite	Group II
Sample:	99041432	02	99080614	(991015–8)	(99080607)	(99080624)	Group II-26)
La	5·95	9·84	9·49	35·93	1·53	1·89	13·60
Ce	9·63	17·84	27·65	152·45	4·63	8·37	36·59
Pr	1·19	1·62	3·38	24·24	0·74	1·51	5·13
Nd	5·22	6·52	12·27	99·13	3·78	8·66	21·23
Sm	3·35	3·22	3·45	32·84	1·44	3·57	5·97
Eu	1·18	1·12	0·92	0·45	0·62	0·91	2·33
Tb	0·98	0·56	0·84	7·13	0·36	0·83	1·17
Gd	4·42	2·92	4·32	36·41	1·76	4·31	6·17
Dy	8·53	4·53	6·23	40·79	3·15	6·46	6·23
Ho	1·71	1·12	1·18	5·38	0·56	1·17	0·96
Er	4·24	2·98	3·38	10·76	1·78	3·50	2·91
Tm	0·58	0·45	0·46	1·18	0·25	0·51	0·38
Yb	3·19	2·57	2·11	7·65	1·14	2·19	1·60
Lu	0·53	0·37	0·35	1·54	0·18	0·37	0·27
Ti	2827	2935	4498	1802	2194	4220	5056
Sr	46·9	41·9	6·19	4·84	54·5	5·79	9·77
Zr	34·9	43·7	57·1	35·5	22·9	53·5	48·8
Y	40·1	24·4	29·1	198·3	15·2	27·1	36·4
La/Yb	1·869	3·831	4·713	4·698	1·350	0·866	8·484
Ti/Zr	80·934	67·219	78·884	50·747	95·865	78·904	103·712
Sr/Y	1·167	1·720	0·209	0·124	3·591	0·215	0·268

orthopyroxenes (Fig. 6). Orthopyroxene around the quartz diorite vein has extremely low values of Al_2O_3 (0·84–2·48 wt.%), Cr_2O_3 (0–0·26 wt.%), CaO (0·28–0·64 wt.%) and Mg# (85·7–90·2). In the thickest wall orthopyroxenite, one can recognise a chemical gradient from the contact with the interior quartz diorite (Mg#=86·3) to the outer contact (Mg#=90·3) with host peridotite, where the Mg# is the same as that of host peridotite olivine. Individual orthopyroxene grains in wall orthopyroxenite often show chemical zoning; for example; the Al_2O_3 content increases from the core (=2·48 wt.%) to the rim (=0·84 wt.%).

4.4. Plagioclase

Plagioclase in the thin, quartz-free veins is relatively constant in composition, showing $An_{49–57}$ [An=100*Ca/(Ca+Na) atomic ratio] and 0·08–0·22 wt.% of K_2O. Plagioclase in the quartz diorite vein has a relatively wide compositional range, from An_{37} to An_{58}. It often shows remarkable zoning when it is in contact with glass (Fig. 7); namely, An content decreases from the core to the mantle, but increases again towards the rim (=contact with glass).

4.5. Hydrous minerals (amphibole and phlogopite)

Amphibole is pargasite in the veins, and is kaersutite in composite xenoliths and Group II. The values of Mg# for pargasite and phlogopite in the veins are 89·0–91·7 and 87·0–91·0, respectively. The hydrous minerals in the veins are higher in Mg# than those of Group II (77·4–84·7 and 66·2–78·9 wt.%, respectively) and related composite xenoliths (71·6–88·8 for pargasite and 66·2–91·3 for phlogopite). Hydrous minerals clearly have higher contents of TiO_2 in Group II and related composite xenoliths than in the veins (=0·81–1·96 wt.%).

4.6. Glass

It is noteworthy that the glass (Table 2) is high in MgO, SiO_2 and Mg#, as compared with slab-derived melts in mantle xenoliths (Schiano *et al*. 1995; Kilian & Stern 2002), typical adakites (Martin 1999), TTG and Phanerozoic Na-rich granitoids (Smithies 2000), and plots off the 'mantle AFC' trend of slab melts on the MgO- SiO_2 diagram (e.g. Smithies 2000). The glass also has low Al_2O_3 and Na_2O contents relative to slab-derived melts (Schiano *et al*. 1995; Kilian & Stern 2002).

4.7. Bulk composition of the quartz diorite vein

The present authors calculated the bulk chemical composition of the quartz diorite vein based on the modal composition (Table 1) and the averaged composition of each phase (Table 2). The quartz diorite vein is rich in Al_2O_3 and CaO, and depleted in Na_2O and K_2O relative to the average adakite and high Al-TTG (Table 4).

The trace element composition of the quartz diorite vein is listed in Table 4. The La/Yb ratio of the quartz diorite vein is about 37·9, and is higher than that of the average adakite, and lower than those of high-Al TTG (Drummond *et al*. 1996) and Phanerozoic Na-rich granitoids (Smithies 2000). The Sr/Y ratio is apparently lower in the vein than in adakite, TTG and Phanerozoic Na-rich granitoids (Table 4).

The quartz diorite vein is characterised by a strongly fractionated REE pattern with a negative Eu anomaly (Fig. 8a). This pattern is similar to those of adakites and TTG, except for the negative Eu spike of the former (Fig. 8a). The quartz diorite vein normalised by primitive mantle abundances shows weak negative anomalies of high-field-strength (HFS) elements (Ti, Nb, Zr and Hf), Eu, Sr, Rb and Ba, and enrichment of Th and U (Fig. 8b). It is similar in incompatible element distribution pattern to adakite and TTG, except for Sr: the quartz diorite exhibits a prominent negative Sr anomaly while adakite shows a positive Sr anomaly, and TTG does not show any Sr anomaly (Fig. 8b).

https://doi.org/10.1017/S0263593300001061 Published online by Cambridge University Press

Table 4 The major-element bulk composition calculated by modal and chemical compositions of minerals, and the trace-element composition determined by ICP-MS analysis of a quartz diorite vein, compared with the average adakite and trondhjemite, tonalite and granodiorite (TTG) compositions (Drummond *et al.* 1996). Note that the Sr/Y ratio is lower in the quartz diorite vein than in adakite and TTG.

	Quartz diorite vein (present study)	Adakite (Drummond *et al.* 1996)	TTG (Drummond *et al.* 1996)
Major elements (wt.%)			
SiO_2	62·89	63·89	70·2
TiO_2	0·16	0·61	0·33
Al_2O_3	21·80	17·4	15·74
Cr_2O_3	0·11		
FeO	0·42	4·21	2·56
MnO	0·14	0·18	0·14
MgO	1·52	2·47	1·19
CaO	9·58	5·23	3·17
Na_2O	3·59	4·4	4·87
K_2O	0·30	1·52	1·88
P_2O_5	0·14	0·19	0·12
Total	100·36	100	100
Mg#	86·6	51·1	43·1
Trace elements (p.p.m.)			
Ti	778		
V	29	72	38
Cr	781	54	36
Ga	5		
Rb	2·94	30	50
Sr	66·6	869	495
Y	6·5	9·5	6·8
Zr	42	117	149
Nb	14	8·3	5·4
Cs	0·7	1·19	1·73
Ba	39	485	746
La	18·6	17·5	29·8
Ce	28·2	34·6	51·6
Nd	9·5	20·1	19·9
Sm	1·89	3·1	2·7
Eu	0·44	0·97	0·91
Gd	1·79	2·25	2·14
Tb		0·37	0·25
Dy	1·44	1·43	1·16
Er	0·56	0·76	0·59
Yb	0·5	0·91	0·46
Lu	0·162	0·15	0·19
Hf	1·13	3·5	3·4
Ta	1·9	0·53	0·55
Pb	0·181		
Th	31	3·52	5·98
U	5	0·99	1·13
Sr/Y	10·2	91·5	72·8
La/Yb	37·2	19·2	64·8

4.8. Trace element compositions of clinopyroxenes

Selected clinopyroxenes from spinel and plagioclase peridotites, peridotites with the veins, quartz diorite vein, composite xenolith, and Group II were analysed *in situ* for REEs and Ti, Sr, Zr and Y by SIMS (Table 3; Fig. 9).

The Sr, Zr and Ti contents of clinopyroxene in the peridotites with the veins show compositional ranges similar to those

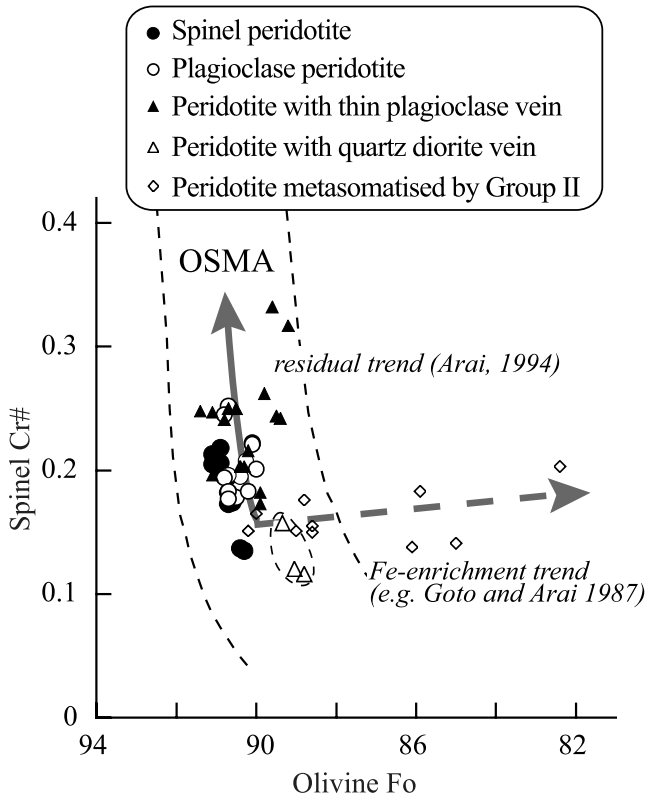

Figure 4 Relationships of the Fo content of olivine and the Cr# [5Cr/(Cr+Al)] atomic ratio of spinel in Tallante peridotite xenoliths. The olivine-spinel mantle array (OSMA), is a spinel peridotite restite trend in terms of the Fo-Cr# relation (Arai 1994). The Fe-enrichment trend shows the metasomatism by Fe-rich melt (Goto & Arai 1987).

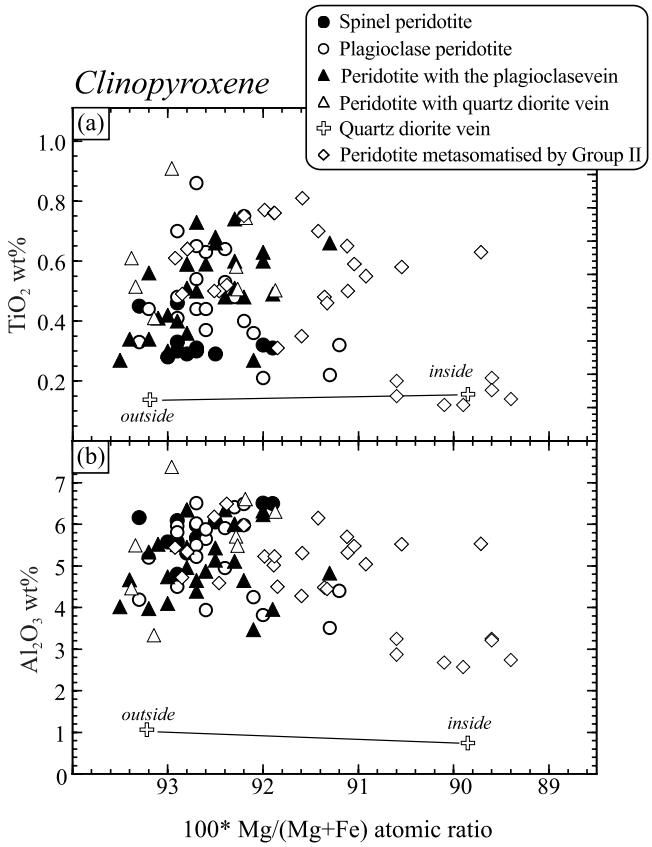

Figure 5 Relationships between TiO_2 and Al_2O_3 content and Mg# [=100*Mg/(Mg+Fe) atomic ratio] in clinopyroxenes in the Tallante peridotite xenoliths, SE Spain. Note that clinopyroxene in quartz diorite vein is distinctively low in Ti and shows a clear chemical zoning in Mg#.

https://doi.org/10.1017/S0263593300001061 Published online by Cambridge University Press

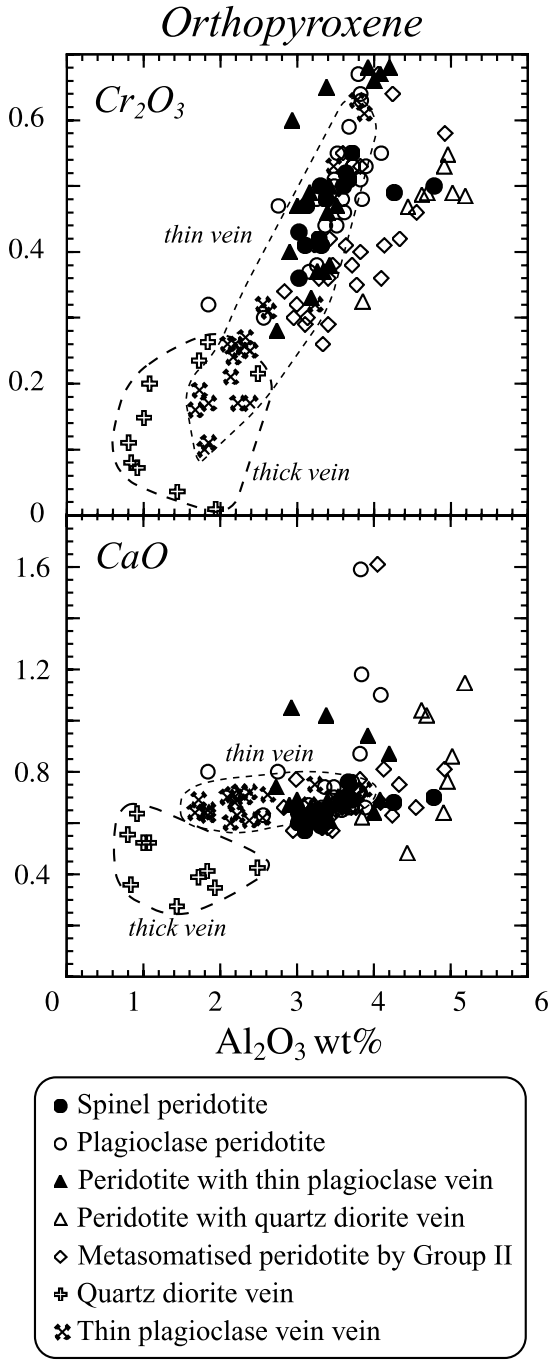

Figure 6 Relationships between the CaO, Cr_2O_3 and Al_2O_3 content of orthopyroxenes in Tallante peridotite xenoliths, SE Spain. Note that orthopyroxene of the thick vein (quartz diorite) is very low in these components and becomes enriched in them to approach mantle orthopyroxene in chemistry with a decrease in the size of the vein.

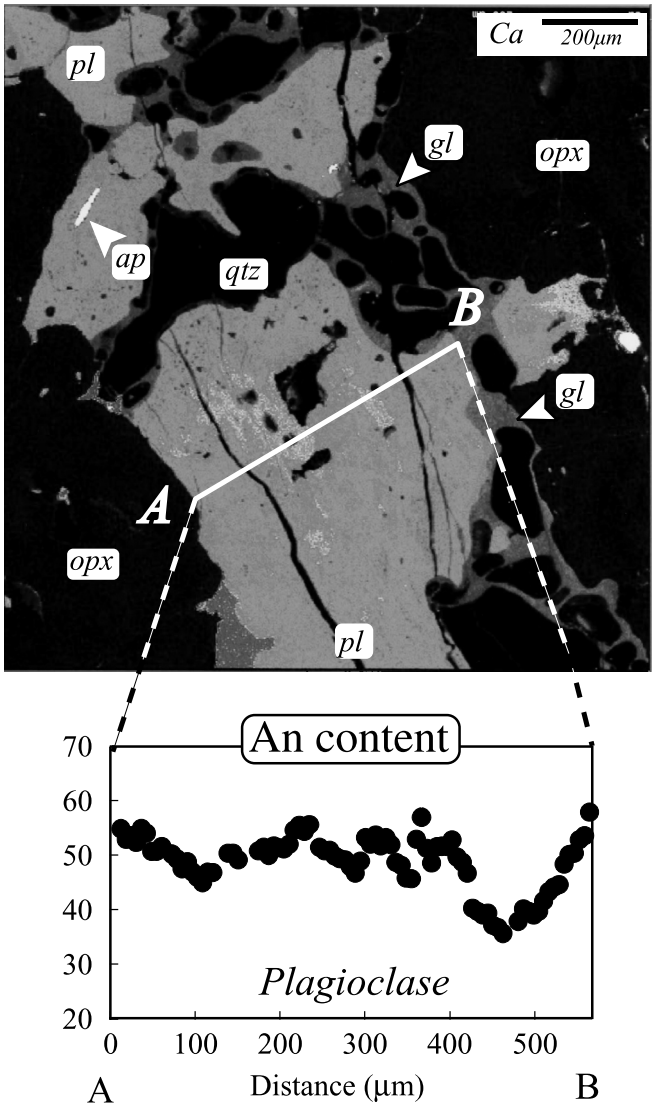

Figure 7 Compositional profile for a plagioclase grain in a quartz diorite vein (Ca compositional map by microprobe). Note that An content decreases from the core to the mantle, but increases again toward the rim (=contact with glass): (pl) plagioclase; (ap) apatite; (gl) glass; (opx) orthopyroxene; and (qtz) quartz.

in vein-free spinel and plagioclase peridotites. The La/Yb ratio of clinopyroxene is relatively higher (=1·9–4·7) in the peridotite with the vein than in spinel peridotite (=1·3–2·3) and plagioclase peridotite (=0·8–1·9). The REE contents of clinopyroxene are generally similar and the chondrite-normalised patterns are flat (Fig. 9). It is noticeable that clinopyroxene is remarkably enriched in LREE (especially, La and Ce) in peridotites with the veins (Fig. 9).

Clinopyroxene in the quartz diorite vein is apparently different from peridotite clinopyroxene in chemistry (Fig. 9). It is characterised by a high content of Y (=198 p.p.m.) and low contents of Ti (=1801 p.p.m.) and Sr (=4·8 p.p.m.) (Table 3). Thus, the Sr/Y ratio is extremely low (Sr/Y=0·024), although the La/Yb ratio is relatively high (=4·7) (Table 3). It has remarkably high REE contents except for Eu (Fig. 9; Table 3). The REE distribution pattern for the quartz diorite clinopyroxene demonstrates a prominent Eu negative spike (Fig. 9).

5. Discussion

The presence of modal quartz in the vein within mantle peridotite xenoliths from Tallante is direct evidence for the activity of silica-oversaturated melt within the upper mantle. The orthopyroxenite intervening between the quartz diorite and host peridotite indicates that it is a reaction product between a slilica-oversaturated melt and host olivine. This is consistent with orthopyroxene chemistry (Fig. 6): orthopyroxene as a reaction product of the vein approaches peridotite orthopyroxene composition with decreases in the size of vein (Fig. 6). When the veins are thin, the melt/wall rock ratio is low and the silica-oversaturated character of the melt is not preserved. The preservation of quartz only in the centre of the vein indicates that the reaction which consumes the SiO_2 component did not reach completion in a large melt conduit. It may also mean that the orthopyroxene, which can be in equilibrium with both olivine and silica-oversaturated melt, helps, to some extent, keep the silica-oversaturated within the

https://doi.org/10.1017/S0263593300001061 Published online by Cambridge University Press

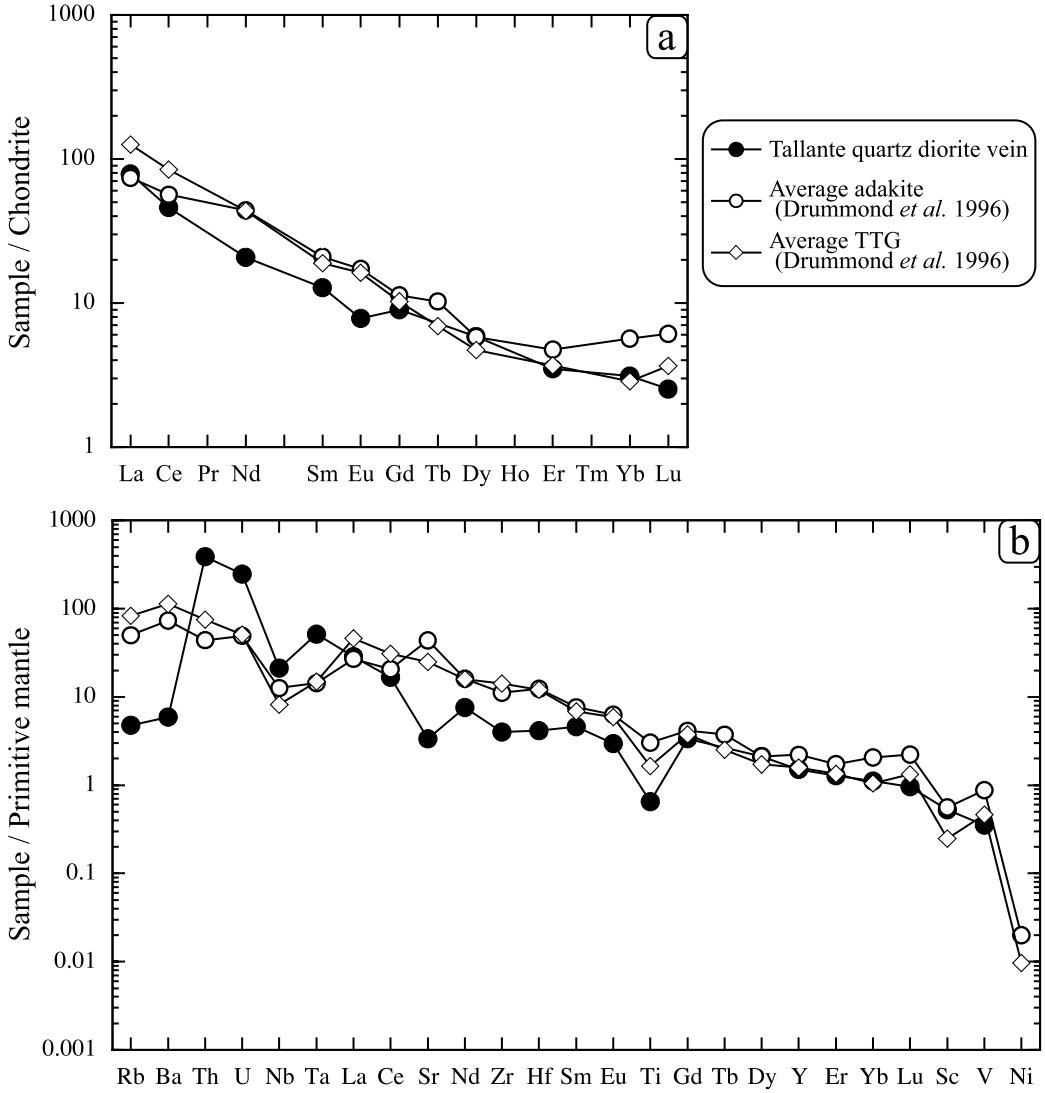

Figure 8 (a) Chondrite (McDonough & Sun 1995) normalised rare-earth element patterns and (b) primitive mantle (McDonough & Sun 1995) normalised trace element distribution patterns of the Tallante quartz diorite vein, adakite and trondhjemite, tonalite and granodiorite (TTG). The quartz diorite vein is similar to adakite and TTG (Drummond *et al.* 1996), except for its negative anomalies of Rb, Ba, Eu and Sr, and positive anomalies of Th and U.

olivine-rich environment. These observations and interpretations suggest that the silica-oversaturated melt can erupt on the Earth's surface only if the melt/wall rock ratio is high within the mantle wedge and/or the orthopyroxene armour is thick enough to work effectively. Kepezhinskas *et al.* (1995) also reported a fine-grained adakitic vein composed of quartz, feldspar, amphibole, Fe-Ti oxide and glass in a mantle peridotite xenolith from the north Kamchatka arc. However, the Kamchatka vein is very fine-grained and has no orthopyroxenite lining, indicating that it has been quenched and provides no information on the behaviour of silica-oversaturated melt within the mantle. The formation of orthopyroxene by the reaction between Si-rich melts and mantle olivine may contribute to Si-enrichment of the mantle wedge (e.g. Kelemen *et al.* 1998).

There are two possibilities for the origin of silica-rich melt within the mantle peridotite. One is the low degree of partial melting of mantle periodtite (e.g. Schiano & Clocchiatti 1994; Baker *et al.* 1995; Hirschmann *et al.* 1998; Schiano *et al.* 1998). However, low-degree partial melt is generally known to occur as inclusions of mantle minerals (e.g. Takahashi 1997; Schiano *et al.* 1998), and this is, therefore, not the case for the Tallante quartz diorite vein that cuts and replaces the host periodtite (Figs 2 & 3). The content of total alkalis in the quartz diorite vein is also very low, while the low-degree partial melt is high in total alkalis (Schiano & Clocchiatti 1994; Baker *et al.* 1995; Hirschmann *et al.* 1998). The other possibility is a derivation from partial melting of the oceanic slab (e.g. Schiano *et al.* 1995; Kepezhinskas *et al.* 1995; Kilian & Stern 2002). This is consistent with the petrochemical characteristics of Tallante quartz diorite vein. It is similar in REE and incompatible trace element abundances to adakite and to TTG (Fig. 8). However, it is noteworthy that the Tallante quartz diorite exhibits a negative Eu anomaly (Fig. 8), indicating precipitation of plagioclase at deeper levels. Plagioclase precipitation is plausible because the Tallante mantle peridotite was derived from the stability field of plagioclase of the shallowest upper mantle (<10 kbar; Kushiro & Yoder 1966). Subtraction of some phases including phlogopite, amphibole and rutile may be necessary because the quartz diorite is also poor in TiO_2, K_2O and Na_2O (Table 2), and is lower in Ba, Rb and Sr than adakite and TTG (Fig. 8b). The highly silicic glass in the quartz diorite vein (Table 2) has possibly formed by *in situ* partial melting of quartz diorite by heating of host alkali basalt because plagioclase in contact with glass shows a reverse zoning (Fig. 7).

https://doi.org/10.1017/S0263593300001061 Published online by Cambridge University Press

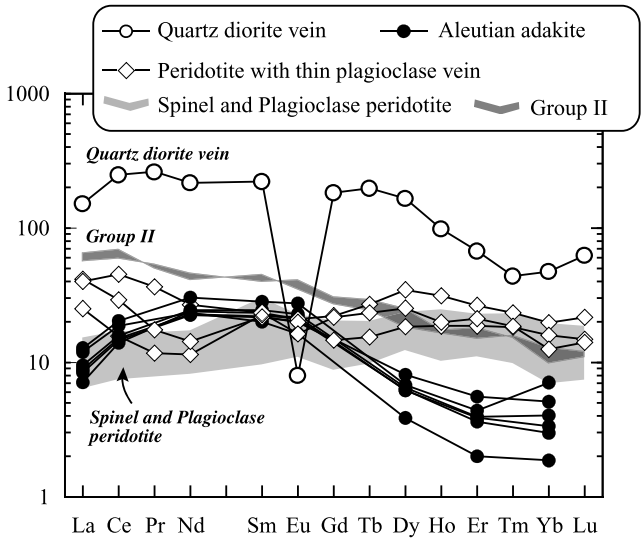

Figure 9 Chondrite-normalised rare-earth element (REE) patterns of selected clinopyrocenes from Tallante mantle xenoliths and clinopyroxene phenocrysts of an adakite from the Aleutian arc (Yogodzinski & Kelemen 1998). The chondrite values are from McDonough & Sun (1995). Note that the clinopyroxene of the quartz diorite vein is apparently higher in REE content than other clinopyroxenes from Tallante. The clinopyroxene of the quartz diorite is very similar in the shape of its REE pattern to that of adakite, except for a negative Eu anomaly. Clinopyroxene from peridotites with the veins shows clear enrichment of LREE compared with other peridotite clinopyroxenes.

The extremely high abundances of REEs of clinopyroxene in the quartz diorite relative to other clinopyroxenes from peridotites and Group II pyroxenites (Fig. 9) clearly indicate the exotic nature of the quartz diorite. The shape of REE pattern in the quartz-diorite clinopyroxene is strikingly similar to that in clinopyroxene phenocrysts in an adakite from the Aleutians (Yogodzinski & Kelemen 1998), except for the prominent negative Eu anomaly of the former (Fig. 9). This is consistent with precipitation of the Tallante clinopyroxene from an adakite melt highly fractionated by precipitation of large amount of plagioclase, which is poor in REEs except for Eu.

The adakitic melt of Tallante may have been derived from a detached slab that is sinking within the asthenospheric mantle beneath the Betic area (Blanco & Spakman 1993; Zeck 1996). Heating of the sinking slab by high-temperature asthenosphere thus produced the adakitic melt.

6. Conclusions

White veins have been commonly found in peridotite xenoliths from Tallante, SE Spain. The thick veins (>1 mm, up to 8 mm) have quartz diorite lithology, and the thinner examples consist only of plagioclase. Orthopyroxene intervenes between the vein (plagioclase ± quartz) and host olivine, indicating an interaction between a silica-oversaturated melt and mantle olivine. The silica-oversaturated character of slab-derived melts can be preserved if the melt/wall olivine ratio is sufficiently high and the orthopyroxene armour works effectively.

The quartz diorite vein from Tallante has adakitic geochemical signatures. Its clinopyroxene is remarkably similar to phenocryst clinopyroxene in adakite from the Aleutians in REE distribution pattern, except for one-order higher abundances of REEs and the strong negative spike of Sr of the former. This feature was obtained by coprecipitation of clinopyroxene and large amounts of plagioclase from an adakitic melt within a confined conduit within the upper mantle, and Tallante quartz diorite is a frozen melt of fractionated adakite affinity. The adakitic melt of Tallante was produced by partial melting of a detached and sinking slab beneath the Betic area in Tertiary times.

7. Acknowledgements

We are indebted to J. Uesugi, M. Kida and C. Tanaka for their assistance in the field. TM is greatly indebted to Steve Eggins, Mike Shelley and Charlotte Allen, Australian National University (ANU), for their guidance in LA-ICP-MS analysis at the ANU. We thank A. Ishiwatari and A. Toramaru for daily discussions. Critical reviews by M. Arima and A. Castro were helpful in revising the manuscript.

This study was partly financed by the 21st Century COE project 'Environmental Monitoring and Prediction of Long- and Short-Term Dynamics of Pan-Japan Sea Area: Construction of Monitoring Network and Assessment of Human Effects', led by K. Hayakawa, Kanazawa University, Kanazawa, Japan.

8. References

Ancochea, E. & Nixon, P. H. 1987. Xenoliths in the Iberian Peninsula. *In* Nixon, P. H. (ed.) *Mantle Xenoliths*, 119–25. Chichester: John Wiley & Sons.

Arai, S. 1994. Characterization of spinel peridotites by olivine-spinel compositional relationships: review and interpretation. *Chemical Geology* **111**, 191–204.

Arai, S., Shimizu, Y. & Gervilla, F. 2003. Quartz diorite veins in a peridotite xenolith from Tallante, Spain: implications for reaction and survival of slab-derived SiO_2-oversaturated melt in the upper mantle. *Proceedings of the Japan Academy, Series B* **79**, 145–50.

Araña, V. & Vegas, R. 1974. Plate tectonics and volcanism in the Gibraltar arc. *Tectonophysics* **24**, 197–212.

Baker, M. B., Hirschmann, M. M., Ghiorso, M. S. & Stolper, E. M. 1995. Compositions of near-solidus peridotite melts from experiments and thermodynamic calculations. *Nature* **375**, 308–11.

Blanco, M. J. & Spakman, W. 1993. The P-wave velocity structure of the mantle below the Iberian Peninsula: evidence for subducted lithosphere below southern Spain. *Tectonophysics* **221**, 13–34.

Capedori, S., Venturelli, G., Salvioli-Mariani, E., Crawford, A. J. & Barbieri, M. 1989. Upper-mantle xenoliths and megacrysts in an alkali basalt from Tallante, south-eastern Spain. *European Journal of Mineralogy* **1**, 685–99.

Defant, M. J. & Drummond, M. S. 1990. Derivation of some modern arc magmas by melting of young subducted lithosphere. *Nature* **347**, 662–5.

Drummond, M. S., Defant, M. J. & Kepezhinskas, P. K. 1996. Petrogenesis of slab-derived trondhjemite-tnalite-dacite/adakite magmas. *Transactions of the Royal Society of Edinburgh: Earth Sciences* **87**, 205–15.

Dupuy, C., Dostal, J. & Boivin, P. A. 1986. Geochemistry of ultramafic xenoliths and their host alkali basalts from Tallante, southern Spain. *Mineralogical Magazine* **50**, 231–9.

Frey, F. A. & Prinz, M. 1978. Ultramafic inclusions from San Carlos, Arizona: petrologic and geochemical data bearing on their petrogenesis. *Earth and Planetary Science Letters* **38**, 129–76.

Goto, K. & Arai, S. 1987. Petrology of peridotite xenoliths in lamprophyre from Shingu, southwestern Japan: implications for origin of Fe-rich mantle peridotites. *Mineralogy and Petrology* **37**, 137–55.

Hirschmann, M. M., Barker, M. B. & Stolper, E. M. 1998. The effect of alkalis on the silica content of mantle-derived melts. *Geochimica et Cosmochimica Acta* **62**, 883–902.

Irving, A. J. 1980. Petrology and geochemistry of composite ultramafic xenoliths in alkali basalts and implications for magmatic processes within the mantle. *American Journal of Science* **280–A**, 389–426.

Kay, S. M., Ramos, V. A. & Marques, M. 1993. Evidence in Cerro Pampa volcanic rocks for slab-melting prior to ridge collision in southern South America. *Journal of Geology* **101**, 703–14.

Kelemen, P. B. 1995. Genesis of high Mg# andesites and the continental crust. *Contributions to Mineralogy and Petrology* **120**, 1–9.

Kelemen, P. B., Hart, S. R. & Bernstein, S. 1998. Silica enrichment in the continental upper mantle via melt/rock reaction. *Earth and Planetary Science Letters* **164**, 387–406.

https://doi.org/10.1017/S0263593300001061 Published online by Cambridge University Press

Kepezhinskas, P. E., Defant, M. J. & Drummond, M. S. 1995. Na metasomatism in the island-arc mantle by slab melt-mantle interaction: evidence from mantle xenoliths in the North Kamchatka. *Journal of Petrology* **36**, 1505–27.

Kilian, R. & Stern, C. R. 2002. Constraints on the interaction between slab melts and the mantle wedge from adakitic glass in peridotite xenoliths. *European Journal of Mineralogy* **14**, 25–36.

Kushiro, I. & Yoder, H. S. 1966. Anorthite-forsterite and anorthite-enstatite reactions and their bearing on the basalt-eclogite transformation. *Journal of Petrology* **7**, 337–62.

López, S. & Castro, A. 2001. Determination of the fluid-absent solidus and supersolidus phase relationships of MORB-derived amphibolites in the range 4–14 kbar. *American Mineralogist* **86**, 1396–403.

López-Ruiz, J. & Rodoríguez-Badiola, E. 1980. La región volcánica Neógena del sureste de Espãna. *Estudios Geológicos* **36**, 5–63.

Martin, H. 1999. Adakitic magmas: modern analogues of Archaean granitoids. *Lithos* **46**, 411–29.

McDonough, W. F. & Sun., S.-S. 1995. The composition of the Earth. *Chemical Geology* **120**, 223–53.

Mercier, J.-C. C. & Nicolas, A. 1975. Textures and fabrics of upper mantle peridotites as illustrated by xenoliths from basalts. *Journal of Petrology* **16**, 454–87.

Rapp, R. P., Watson, E. B. & Miller, C. F. 1991. Partial melting of amphibolite/eclogite and the origin of Archean trondhjemites and tonalites. *Precambrian Research* **51**, 1–25.

Rapp, R. P., Shimizu, N., Norman, M. D. & Applegate, G. S. 1999. Reaction between slab-derived melts and peridotite in the mantle wedge: experimental constrains at 3·8 GPa. *Chemical Geology* **160**, 335–56.

Rapp, R. P. & Watson, E. B. 1995. Dehydration melting of metabasalt at 8–32 kbar: implications for continental growth and crust-mantle recycling. *Journal of Petrology* **36**, 981–931.

Rudnick, R. L. & Fountain, D. M. 1995. Nature and composition of the continental crust: a lower crustal perspective. *Reviews of Geophysics* **33**, 267–309.

Schiano, P., Clocchiatti, R., Shimizu, N., Maury, R., Jochum, K. P. & Hofmann, A. W. 1995. Hydrous, silica-rich melts in the sub-arc mantle and their relationships with erupted arc lavas. *Nature* **377**, 595–600

Schiano, P., Buourdon, B., Clocchiatti, R., Massare, D., Varela, M. E. & Bottinga, Y. 1998. Low-degree partial melting trends recorded in upper mantle minerals. *Earth and Planetary Science Letters* **160**, 537–50.

Schiano, P. & Clocchiatti, R. 1994. Worldwide occurrence of silica-rich melts in sub-continental and sub-oceanic mantle minerals. *Nature* **368**, 621–4.

Sen, C. & Dunn, T. 1994. Experimental modal metasomatism of a spinel lherzolite and the production of amphibole-bearing peridotite. *Contributions to Mineralogy and Petrology* **119**, 422–32.

Smithies, R. H. 2000. The Archaean tonalote-trondhjemite-granodiorite (TTG) series is not an analogue of Cenozoic adakite. *Earth and Planetary Science Letters* **182**, 115–25.

Streckeisen, A. 1976. To each plutonic rock its proper name. *Earth Science Reviews* **12**, 1–33.

Takahashi, N. 1997. Incipient melting of mantle peridotites observed in the Horoman and Nikanbetsu peridotite complexes, Hokkaido, northern Japan. *Journal of Mineralogy, Petrology, and Economic Geology* **92**, 1–24.

Tatsumi, Y. 2000a. Continental crust formation by crustal delamination in subduction zones and complementary accumulation of the enriched mantle I component in the mantle. *Geochemistry Geophysics Geosystems* Paper number 2000GC000094.

Tatsumi, Y. 2000b. Slab melting: its role in continental crust formation and mantle evolution. *Geophysical Research Letters* **27**, 3941–4.

Taylor, S. R. & McLennan, S. M. 1985. *The continental crust: its composition and evolution*. Oxford: Blackwell.

Turner, S. P., Platt, J. P., George, R. M. M., Kelley, S. P., Pearson, D. G. & Nowell, G. M. 1999. Magmatism associated with orogenic collapse of the Betic-Alboran domain, SE Spain. *Journal of Petrology* **40**, 1011–36.

Venturelli, G., Mariani, E. S., Foley, S. F., Capedri, S. & Crawford, A. J. 1988. Petrogenesis and crystallization of Spanish lamproitic rocks. *Canadian Mineralogist* **26**, 67–79.

Wang, W. & Yurimoto, H. 1993. Analysis of rare earth elements in garnet by SIMS. *Annual Report of the Institute of Geoscience, the University of Tsukuba* **19**, 87–91.

Yogodzinski, G. M. & Kelemen, P. B. 1998. Slab-melting in the Aleutians: implications of an ion probe study of clinopyroxene in primitive adakite and basalt. *Earth and Planetary Science Letters* **158**, 53–65.

Yurimoto, H., Yamashita, A., Nishida, N. & Sueno, S. 1989. Quantitative SIMS analysis of GSJ rock reference samples. *Geochemical Journal* **23**, 215–36

Zeck, H. P. 1996. Betic-Rif orogeny: subduction of Mesozoic Tethys lithosphere under eastward drifting Iberia, slab detachment shortly before 22 Ma, and subsequent uplift and extensional tectonics. *Tectonophysics* **254**, 1–16.

Y. SHIMIZU, S. ARAI and T. MORISHITA, Graduate School of Natural Science and Technology, Kanazawa University, Kakuma-machi, Kanazawa 920-1192, Japan.

H. YURIMOTO, Department of Earth and Planetary Sciences, Faculty of Science, Tokyo Institute of Technology, 2-12-1 Ookayama, Meguro-ku, Tokyo 152–8550, Japan.

F. GERVILLA, Instituto Andaluz de Ciencias de la Tierra, University of Granada-C.S.I.C., Fuentenueva S/N, E-18002, Granada, Spain.

MS received 2 October 2003. Accepted for publication 7 September 2004.